Applied Catalysis B: Environmental 98 (2010) 1–9

Contents lists available at ScienceDirect

Applied Catalysis B: Environmental

journal homepage: www.elsevier.com/locate/apcatb

Review

Direct hydrazine fuel cells: A review

Alexey Serov*, Chan Kwak

Corporate R&D Center, Samsung SDI, Shin-dong 575, Yeongtong-gu, Suwon-si, Gyeonggi-do 443-731, South Korea

ARTICLE INFO

Article history:
Received 27 February 2010
Received in revised form 27 April 2010
Accepted 1 May 2010
Available online 9 May 2010

Keywords:
Hydrazine oxidation
Fuel cell
Anode
Catalyst

ABSTRACT

Low-temperature fuel cells operating on hydrazine fuel in acid and alkaline media comprise a promising class of new, non-conventional sources of energy. High battery performance is expected of hydrazine-based cells. The electrooxidation of hydrazine on the surface of different catalysts has been extensively studied recently. Examples of Direct Hydrazine Fuel Cells (DHFC) with anion or cation-exchange membranes show notable power densities. These aspects of DHFC development with analysis of future improvements in their performance based on changes such as an increase in catalytic activity, membrane type selection and MEA fabrication, are summarized in the present review.

Contents

1. Introduction 1
2. Development of catalysts for electrooxidation of hydrazine 2
3. MEA fabrication and DHFC performance 6
4. Conclusions 9
References 9

1. Introduction

Recently, several companies have started to supply power sources based on fuel cell technology to the market. The possible applications of fuel cells are wide, from mobile devices to automobiles and space ships. At the moment, one of the main focus of fuel cell research is portable devices, such as mobile phones, mp3 players and notebooks. This type of fuel cell is usually powered by liquid fuels, such as alcohols (direct alcohol fuel cells) [1–22], simplest ethers (direct dimethyl ether fuel cells) [23–36] or organic acids (direct formic acid fuel cells) [37].

An analysis of open source data (scientific publications, company's press-releases, "white papers", etc.) shows that Direct Methanol Fuel Cells (DMFCs) are the closest to commercialization among all directly fed fuel cells. However, DMFCs still have a number of drawbacks, including the usage of high amounts of platinum as anode and cathode catalysts, resulting in an extremely high price for the final devices, and methanol crossover from anode to cathode through cation-exchange membranes, significantly decreasing the FC performance and fuel cell durability.

The problem of high costs can be solved by using non-platinum anode and cathode materials [38–43]. The studies in this field lead the choice of catalysts to be restricted to those with activity similar to platinum/platinum-based alloys but that are significantly cheaper, more tolerant to methanol crossover, and simpler to manufacture. Methanol crossover can be decreased by using either an anion-exchange membrane or a modified cation-exchange membrane. In summary, the DMFCs can be considered conventional fuel cells.

However, investigation of new types of low-temperature liquid-fed fuel cells based on alternative fuels, such ethylene glycol [44], sodium borohydride [45] and hydrazine [46–72], show promising results.

Hydrazine as a fuel for alkaline fuel cells has been studied since the 1970s [67,68]. The reasons for considering hydrazine as a promising fuel are:

- its electrooxidation produces no CO_2, reducing the overall emission of greenhouse gases,

* Corresponding author at: Paul Scherrer Institute, Radiochemistry (LCH), PSI OFLB/105, 5232 Villigen PSI, Switzerland. Tel.: +41 56 5345251; fax: +41 56 3104435.
E-mail addresses: alexey.serov@psi.ch, vores@mail.ru (A. Serov), kcpmhkj@yahoo.com (C. Kwak).

0926-3373/$ – see front matter © 2010 Elsevier B.V. All rights reserved.
doi:10.1016/j.apcatb.2010.05.005

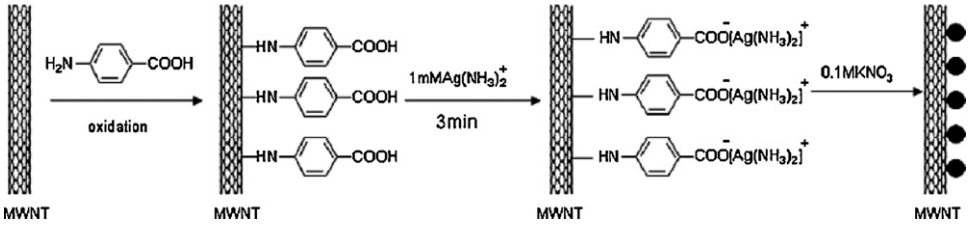

Fig. 1. Schematic procedure for the preparation of Ag nanoparticles on MWNT surface. Reproduced from [49] with permission from Elsevier.

- the absence of carbon atoms in hydrazine leads to zero production of species that may poison the electrocatalysts (e.g., CO and products of incomplete C_2-molecules oxidation),
- the theoretical electromotive force is relatively high, with a value of 1.56 V [69], which results in high power density.

On the other side, the high toxicity of hydrazine should be taken into account during the design of complete system to prevent any contact of customers with fuel (either from fuel tank or with unreacted one). Recently Daihatsu Motor has developed a method for safe storage of hydrazine in fuel tanks as a solid hydrazone form (>C=N–NH_2) [72]. This form does not exhibit mutagenic properties as well as its solid nature is much safer compared to liquid hydrazine in case of tank damage. The hydrazine can be released from its hydrazone form by adding solvent into the fuel tank [72].

This review is devoted to the analysis of recent developments in the electrooxidation of hydrazine on different catalysts, the investigation of membrane type influence on fuel cell performance and MEA fabrication.

2. Development of catalysts for electrooxidation of hydrazine

The total reaction of hydrazine electrooxidation can be written as:

$$N_2H_4 + O_2 \rightarrow N_2 + 2H_2O, E_0 = 1.56\,V \quad (1)$$

Hydrazine–water solutions easily undergo hydrolysis, producing the hydrazonium cation:

$$N_2H_4 + H_2O = N_2H_5^+ + OH^- \quad (2)$$

It is possible to oxidize N_2H_4 both in acidic and alkaline media by the following reactions:

$$N_2H_5^+ \rightarrow N_2 + 5H^+ + 5e^- (acid) \quad (3)$$

$$N_2H_4 + 4OH^- \rightarrow N_2 + 4H_2O + 4e^- (alkaline) \quad (4)$$

Operation of fuel cells in acidic conditions requires catalysts based on stable, non-corrosive noble metals, usually platinum or platinum-group metals. However, cheaper noble metals (Ag, Pd, etc.) [49,51–54,57–59] and even base metals (Cu, etc.) [62] can be used in alkaline-type direct hydrazine fuel cells.

Recently, a number of silver catalysts have been prepared by different methods and evaluated for electrooxidation of hydrazine [49,51,52,57]. Li and co-workers investigated the deposition of Ag nanoparticles on the surface of carbon nanotubes by electrochemical [49] and ultrasound methods [52]. Fig. 1 shows a scheme of electrochemical synthesis of Ag/CNT. Electrochemical measurements show high catalytic activity of prepared composite material to the electrooxidation of hydrazine (Fig. 2). The relationship between the peak currents, obtained from the CV scan and $v^{1/2}$ of CV (inset of Fig. 2), is linear, which results in the conclusion that the oxidation of hydrazine is controlled by a diffusion process. The reduction of $AgNO_3$ under ultrasound irradiation in the presence of benzyl mercaptan and dispersed CNT results in controllable

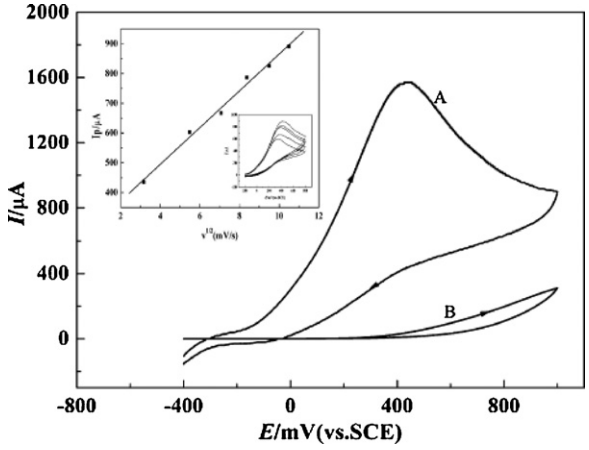

Fig. 2. Cyclic voltammograms of 10 mM $N_2H_4 \times H_2O$ in 0.1 M K_2SO_4 solution at the Ag/MWNT electrode (A) and bare MWNT electrode (B). Scan rate: 100 mV s^{-1}. Inset: Ip vs. $v^{1/2}$ plot of cyclic voltammograms of 10 mM $N_2H_4 \times H_2O$ in 0.1 M K_2SO_4 solution at the Ag/MWNT electrode (scan rate 30, 50, 70, 90, and 110 mV/s). Reproduced from [49] with permission from Elsevier.

deposition of Ag nanoparticles on the surface of CNTs [52]. By controlling the silver loading on supported material, catalysts with Ag wt% of 10, 20, 40 and 60 were prepared. CV curves of hydrazine oxidation on Ag/CNT catalysts with different loadings are shown in Fig. 3. The authors confirmed their suggestion that electrooxidation of hydrazine is controlled by diffusion processes [49]. The catalytic activity of Ag/CNT with the highest loading (60 wt%) was lower than expected (Fig. 3 inset) due to silver particle agglomeration on the surface of CNTs. The methods of preparation of Ag/CNT suggested by the authors are simple and permit control of particle

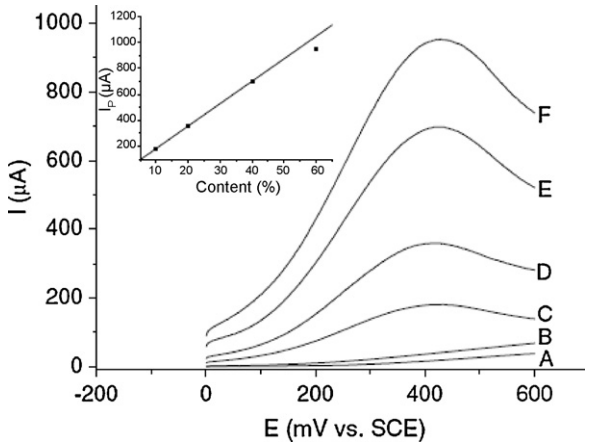

Fig. 3. CV curves of 10 mM hydrazine in 0.1 M K_2SO_4 solution. Bare GC electrode (A), pristine MWCNTs modified GC electrode (B) and Ag/CNT modified GC electrode with different Ag catalyst content: (C) 10%, (D) 20%, (E) 40%, and (F) 60%. Inset: plots of peak current (Ip) against Ag catalyst content in Ag/CNT composite. Scan rate: 100 mV s^{-1}. Reproduced from [52] with permission from Elsevier.

morphology as well as catalyst loading. The high activity of prepared electrocatalysts should be examined in further experiments with MEA performance.

Another simple method of preparation of silver nanoparticles deposited on the carbon black (CB) by mixing surface-functionalized CB with Ag colloid particles was suggested by Wang and co-workers [57]. The prepared catalyst can be characterized by homogeneous particle distribution on the surface of a carbon support with particle size ~6 nm. Experiments of hydrazine oxidation on Ag/CB show the well-defined anodic peak of N_2H_4 oxidation at about +0.5 V vs. SHE (Fig. 4). Silver nanoparticles deposited on the Ti support were synthesized by a hydrothermal method, and Ag/Ti catalysts were studied for the electrooxidation of hydrazine in alkaline media [51]. The cyclic voltammograms of the nano-Ag/Ti electrode in 1.0 M NaOH solution containing different hydrazine concentrations are presented in Fig. 5, which shows that the current densities for the reduction peaks C1 and C2 decrease with an increase in hydrazine concentration. The peak C1 completely disappears in the presence of 40 mM N_2H_4 while intensity of the peak C2 becomes lower, indicating that the anodic oxidation of the silver particles is inhibited due to the presence of hydrazine. It is possible to conclude that these results show high activity of the prepared nano-Ag/Ti electrode towards hydrazine oxidation.

Palladium has been studied as a possible electrocatalyst for anode application in DHFCs [53,54,58,59]. Wang and co-workers developed a simple method for the deposition of palladium nanoparticles onto the surface of CNTs using benzyl mercaptan

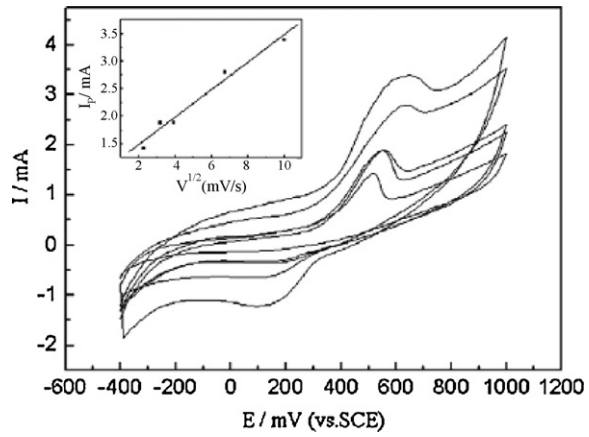

Fig. 4. Cyclic voltammograms for the Ag/CB hybrid catalysts in 10 mM $N_2H_4 \times H_2O$ + 0.1 M K_2SO_4 at sweep rates of 5, 10, 15, 45, and 100 mV s^{-1}. Inset: Ipa ~ $v^{1/2}$ relationship. Reproduced from [57] with permission from Elsevier.

[58] (Fig. 6). The electrochemical performance of the Pd/CNT catalysts was studied for the oxidation of hydrazine; Fig. 7 shows the CV curves of 10 mM $N_2H_4SO_4$ in 0.1 M K_2SO_4 solution over different electrodes. The CV curves show that the palladium deposited on the CNTs is an active catalyst for hydrazine oxidation, but its activity is only comparable with silver catalysts [49]. Dendrimer-encapsulated Pd nanoparticles anchored on carbon nanotubes

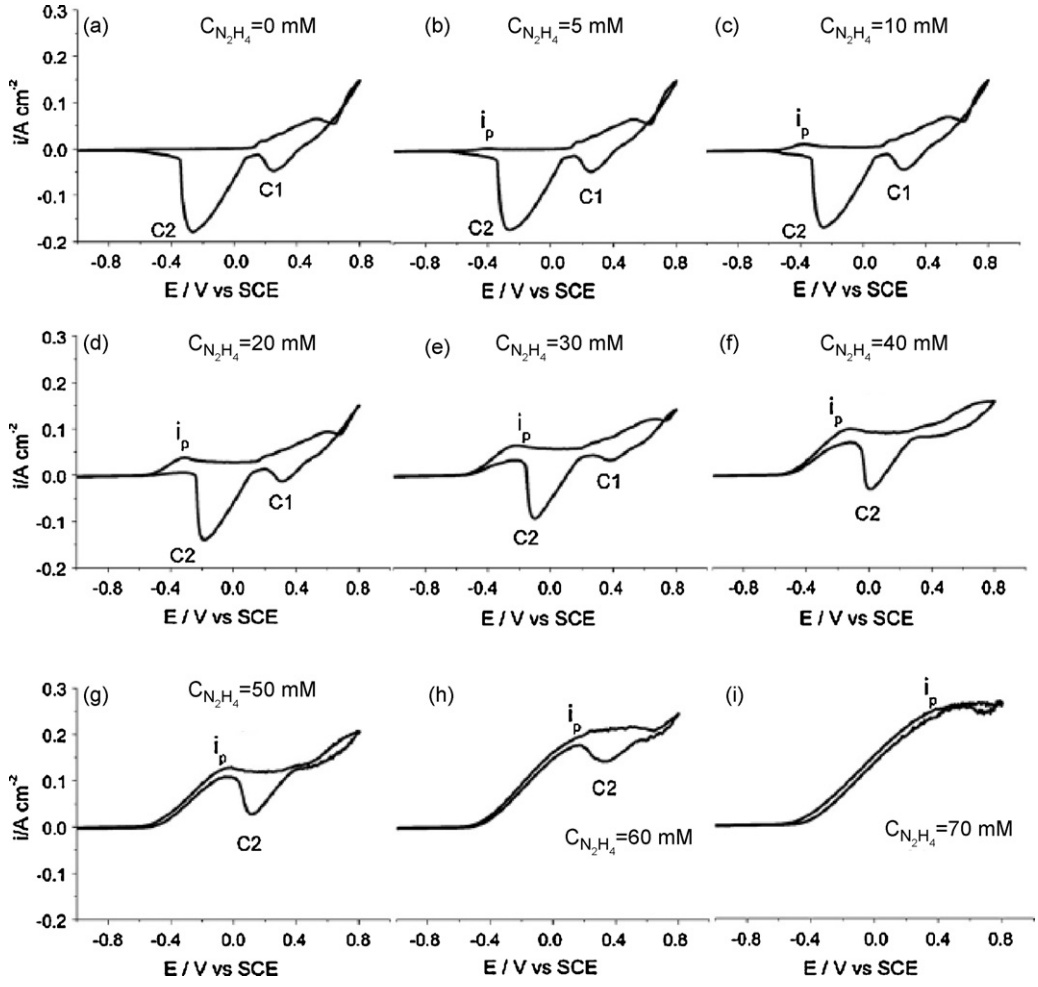

Fig. 5. Cyclic voltammograms of the nano-Ag/Ti electrode at a scan rate of 100 mV/s in the presence of different hydrazine concentrations in 1 M NaOH solution. Reproduced from [51] with permission from Elsevier.

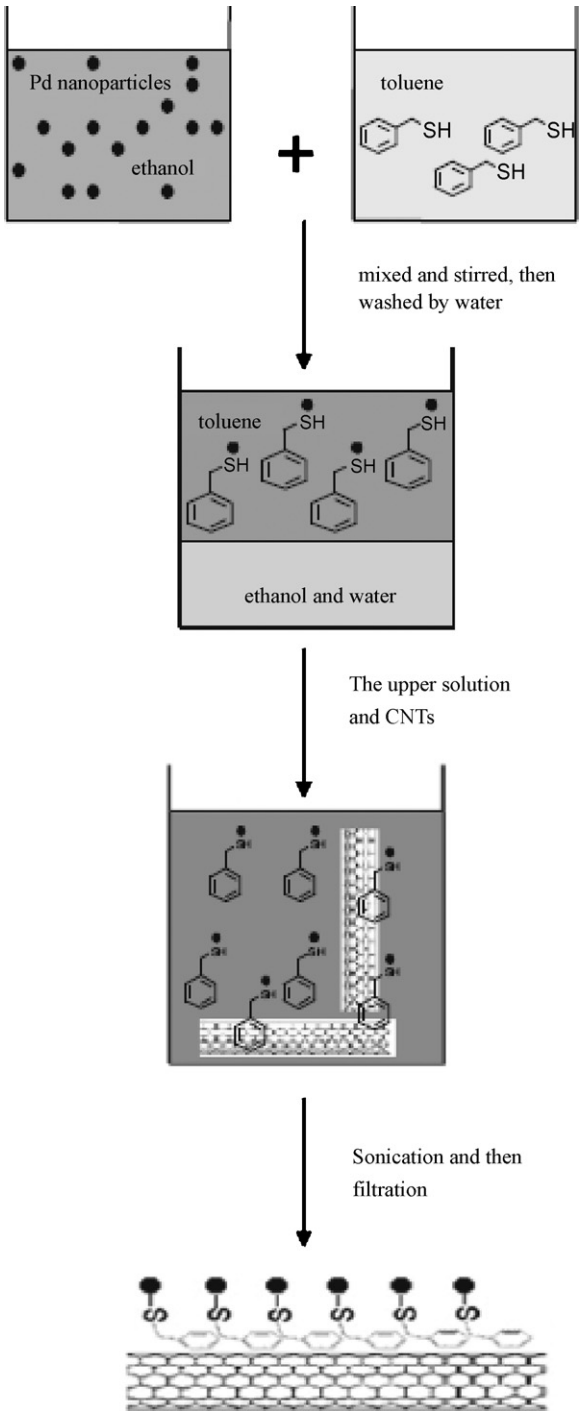

Fig. 6. Schematic illustrations of the synthesis procedures of Pd/CNT catalysts. Reproduced from [58] with permission from Elsevier.

(Pd/G4-NH_2/MWNTs) and their catalytic activities were investigated by [59]. CVs for hydrazine oxidation using a GCE modified with Pd/G4-NH_2/MWNTs, Pd/G4-NH_2, Pd-free G4-NH_2/MWNTs, MWNTs and a bare GCE are shown in Fig. 8. Electrodes modified with palladium show high catalytic activity for hydrazine oxidation with maximal activity for Pd/G4-NH_2/MWNTs. The authors suggested a possible usage of this nanocomposite material as a future anode for DHFC [59]. Comparative studies of the electrooxidation of hydrazine on Pd catalysts electrodeposited on indium tin oxide glass (ITO) and Pd/WO_3 on ITO were performed by Wang and coworkers [53]. The promotion effects of WO_3 are shown in Fig. 9.

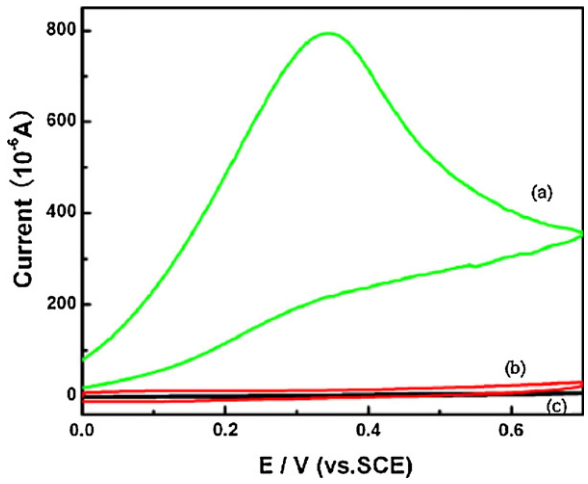

Fig. 7. Cyclic voltammograms of hydrazine oxidation on Pd/CNT catalysts (a), pristine CNTs (b) and bare GC electrode (c) in 10 mM $N_2H_4SO_4$ + 0.1 M K_2SO_4 solution at room temperature. Reproduced from [58] with permission from Elsevier.

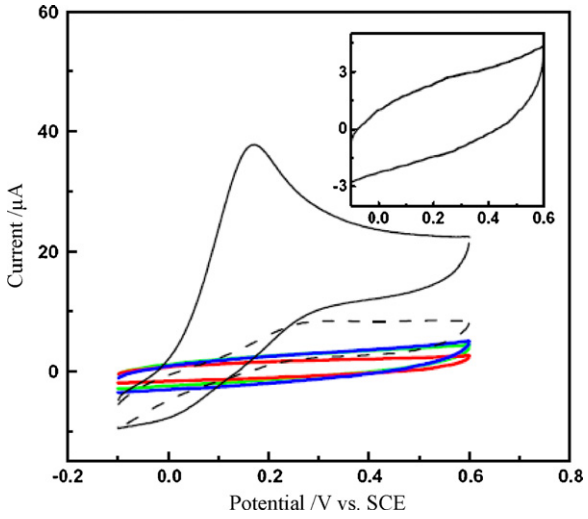

Fig. 8. CVs for hydrazine oxidation using a GCE modified with: Pd/G4-NH2/MWNTs (black straight curve), Pd/G4-NH2 (black dashed curve), Pd-free G4-NH2/MWNTs (blue curve), MWNTs (green curve) and a bare GCE (red curve). 0.1 M KNO3 + 1 mM $N_2H_4SO_4$. Inset: CV of a GCE modified with Pd/G4-NH2/MWNTs in 0.1 M KNO3 solution. Reproduced from [59] with permission from Elsevier. (For interpretation of the references to color in this figure legend, the reader is referred to the web version of the article.).

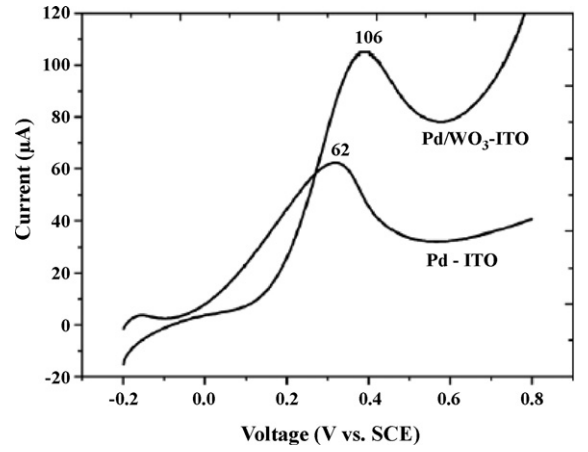

Fig. 9. Comparison of the electrochemical activity of Pd/WO_3-ITO and Pd-ITO electrodes. Scan rate of 100 mV s^{-1}. Electrolyte: 5 mM $N_2H_4SO_4$ and 0.1 M K_2SO_4. Reproduced from [53] with permission from Elsevier.

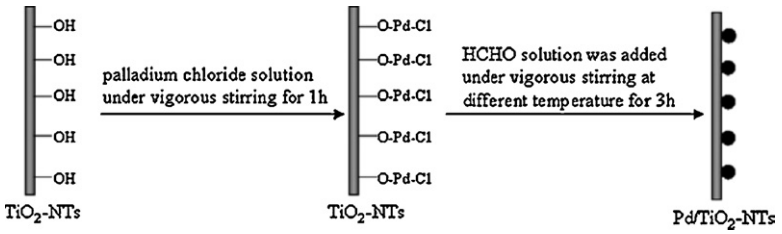

Fig. 10. A schematic diagram showing the steps for the synthesis of Pd/TiO_2-NTs catalysts. Reproduced from [54] with permission from Elsevier.

It is clear from Fig. 9 that the addition of tungsten oxide significantly improves the performance of the electrodes. A peak current of 106 μA was achieved for the Pd/WO_3-ITO electrode, a value 1.7 times higher than that for the Pd-ITO glass electrode (62 μA) [53]. The authors explain the promotional effect of tungsten oxide on the catalytic electrooxidation of hydrazine by the good distribution of palladium nanoparticles on the WO_3 support. Palladium deposited on the TiO_2-nanotubes was synthesized by the reduction of the palladium salt on the dispersed titania nanotubes [54] (Fig. 10). In this case, the electrooxidation of hydrazine was performed on a GC electrode modified with different Pd catalysts by CV. Fig. 11 shows the voltammogram curves of pure TiO_2-NTs, Pd/TiO_2 particles, unsupported Pd and Pd/TiO_2-NTs (10 mM N_2H_4•H_2O in 0.1 M K_2SO_4). Palladium deposited at the TiO_2-nanotubes showed the highest activity towards hydrazine electrooxidation. The authors attributed the obtained results to the higher surface area for titanium oxide nanotubes, which produces better-dispersed palladium nanoparticles of smaller size [54].

The electrooxidation of hydrazine by composite Au-nanoparticles/polypyrrole nanowires (Au/PPy) was studied by Li and Lin [50]. CVs of hydrazine oxidation on Au/PPy/GCE were compared to those obtained on Au/GCE, PPy/GCE and bare GCE in the presence of 5.0×10^{-4} M hydrazine, as shown in Fig. 12. The overall negative shift in peak potential of about 515 mV indicated that the catalytic activity of these electrodes follows the order of Au/PPy/GCE > Au/GCE > PPy/GCE > bare GCE, with gold nanoparticles resulting in high catalytic activity for hydrazine oxidation. An Au/Ti electrode was prepared by the same method as Ag/Ti [51] (see above), and their activity towards hydrazine oxidation was studied [60]. Their results indicated that the electrooxidation of hydrazine on the Au/Ti takes place at the onset potential of −0.55 V, while the onset potential of hydrazine oxidation on the polycrystalline Au is −0.02 V. In addition, the Au/Ti electrode exhibits a much larger anodic current density of hydrazine oxidation than Au electrode.

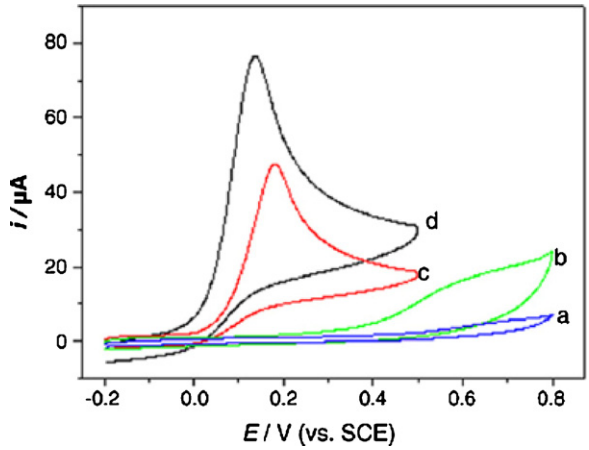

Fig. 12. CVs of 5.0×10^{-4} M hydrazine in 0.1 M PBS (pH 7.0) at bare GCE (a), PPy/GCE (b), Au/GCE (c) and Au/PPy/GCE (d). Scan rate: 50 mV s^{-1}. Reproduced from [50] with permission from Elsevier.

The results show considerable enhancement in electrocatalytic activity of the Au/Ti electrode for hydrazine oxidation compared to that of the polycrystalline Au electrode.

The mechanism and structural sensitivity of hydrazine oxidation in alkaline media on polycrystalline and single-crystal surfaces of platinum were studied by voltammetry and on-line electrochemical mass spectrometry (MS) [55]. This research shows that hydrazine oxidation at platinum electrodes is a diffusion-controlled electrocatalytic mechanism over a wide potential region (Fig. 13). From the onset of the hydrazine oxidation and the position of the main peak, the electrocatalytic activity was deduced to increase in the order Pt(1 1 0) > Pt(1 0 0) > Pt(1 1 1). The kinetic analysis at low overpotentials indicates that hydrazine oxidation on Pt(1 1 0) and Pt(1 1 1) surfaces is limited by electrochemical steps (presumably,

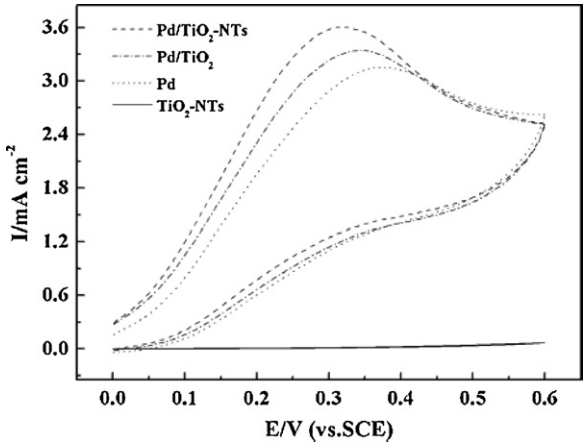

Fig. 11. Cyclic voltammograms of 10 mM $N_2H_4 \times H_2O$ in 0.1 M K_2SO_4 solution at TiO_2-NTs, Pd/TiO_2, unsupported Pd and Pd/TiO_2-NTs electrode. Scan rate: 50 mV s^{-1}. Reproduced from [54] with permission from Elsevier.

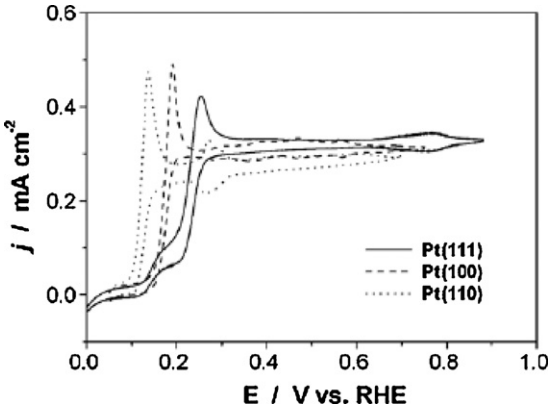

Fig. 13. Electrochemical oxidation of hydrazine at single-crystal platinum electrodes, the voltammetric profiles obtained at Pt(1 1 1), Pt(1 0 0), and Pt(1 1 0) under identical experimental conditions (0.1 M NaOH + 0.82×10^{-3}M N_2H_4; 10 mV s^{-1}). Reproduced from [55] with permission from Elsevier.

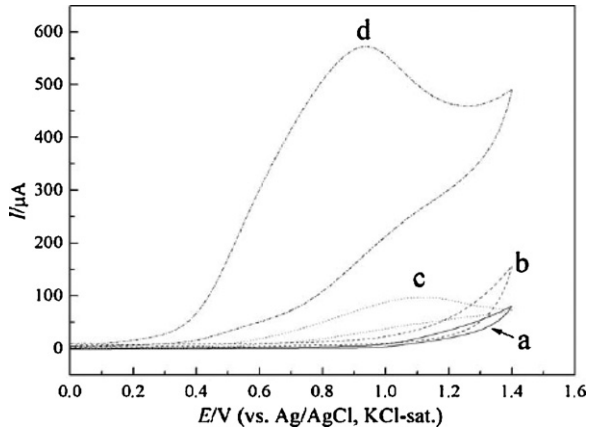

Fig. 14. CVs at the bare GC (a and c) and RGSs/GC electrode (b and d) in the absence (a and b) and in the presence (c and d) of 10 mM hydrazine in 0.1 M KOH solutions at a scan rate of 0.1 V s^{-1}. Reproduced from [64] with permission from Elsevier.

combined electron and proton transfer), whereas on Pt(1 0 0), the chemical step that involves a N_2H_2 intermediate is a likely rate-determining step.

The electrochemical properties of reduced graphene sheets (RGSs) towards hydrazine oxidation in alkaline media were investigated by Zhang and co-workers [64]. The authors compared the catalytic activity of bare GCE and that of a GCE modified by RGS in alkaline media, and they showed that reduced graphene sheets can effectively oxidize hydrazine (Fig. 14). Hydrazine must thus oxidize completely on the surface of reduced graphene sheets, producing only nitrogen [64].

A comprehensive comparative study of the oxidation of hydrazine and its derivatives on the surfaces of different metals (Ni, Co, Fe, Cu, Ag, Au, and Pt) was performed by Asazawa et al. [63]. The voltammograms obtained for the metal electrodes in the hydrazine hydrate solutions are shown in Fig. 15. The onset potentials were 0.654 V for Fe, −0.178 V for Co, −0.108 V for Ni, 0.193 V for Cu, 0.378 V for Ag, 0.384 V for Au, and 0.062 V for Pt. Fig. 15 shows that in the low overpotential region, cobalt possesses higher catalytic activity than platinum. The Fe catalyst, however, is not suitable for operation in the above conditions because it oxidizes. Oxidation of the hydrazine derivatives (methyl carbazate ($N_2H_3COOCH_3$), carbodihydrazide ($N_2H_3CON_2H_3$), hydrazine carbonate ($(N_2H_4)_2CO_2$), and aminopolyacrylamide (APA,–$[CH_2CH(CONHNH_2)]_{0.8}$–$[CH_2CH(CONH_2)]_{0.2}$–) occurred on the surfaces of the studied metals in the low overpotential region, but during the oxidations of carbodihydrazide and methyl carbazate, Platinum exhibits higher catalytic

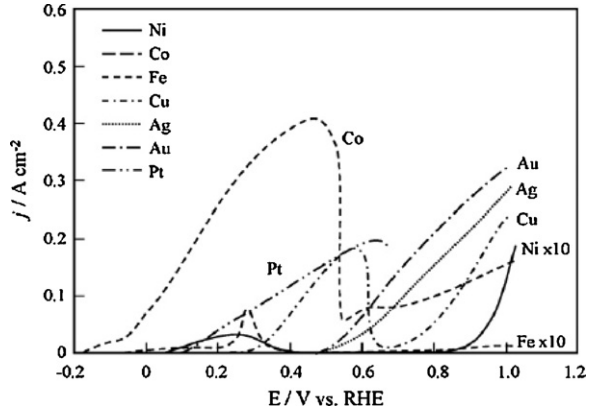

Fig. 15. Oxidation of hydrazine on the metal disk electrodes (5 wt% hydrazine hydrate + 1 M KOH aqueous solution). Sweep rate: 20 mV s^{-1}. Reproduced from [63] with permission from Elsevier.

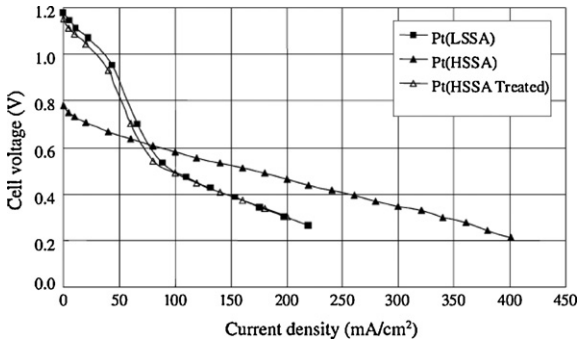

Fig. 16. Effect of Pt-anode catalyst surface area on direct hydrazine fuel cell performance. Specific surface area of anode catalyst: Pt(LSSA) = 7 m^2 g^{-1}, Pt(HSSA) = 35 m^2 g^{-1}, Pt(HSSA heat-treated) = 6.3 m^2 g^{-1}, loading: anode (Pt 2 mg cm^{-2}), cathode (Pt 3 mg cm^{-2}), anode/cathode pressures = 0.1/0.15 MPa. Reproduced from [47] with permission from Elsevier.

activity than Co, as it follows a different mechanism of oxidation from hydrazine [63].

Many researchers have shown that hydrazine can be fully oxidized to produce only nitrogen and water on the surface of many metal catalysts, including non-platinum catalysts that operate in alkaline media. These catalysts possess activity similar to that of Pt but are significantly cheaper. However, certain developments in morphology (particle size and shape) and choice of supports are needed for the non-platinum anode catalysts.

3. MEA fabrication and DHFC performance

The factors affecting the performance of direct hydrazine fuel cells, such as membrane type, anode and cathode catalysts and operation conditions, were studied in several research groups [46–48,56,66]. Yamada et al. investigated the influence of the surface area of platinum catalysts, different membrane types (anion- and cation-exchange) and a number of non-platinum catalysts on the fuel cell performance [46–48]. The dependence of DHFC (using a cation-exchange membrane) performance on the surface area of platinum catalysts is shown in Fig. 16 [47]. At low current densities, catalysts with low surface area (Pt(LSSA)) performed significantly better than those with high surface area (Pt(HSSA)). However, at the current densities higher than 80 mA cm^{-2}, Pt(HSSA) becomes more active. Heat treatment of Pt(HSSA) significantly decreases its surface area from 35 to 6.3 m^2 g^{-1}, and no significant MEA performance difference was observed for Pt(LSSA) and Pt(HSSA heat-treated). To explain this phenomenon, the exhausted gases were analyzed. At the anode side with Pt(LSSA), a large amount of unreacted hydrazine was detected (Fig. 17). The MEAs with Pt(HSSA) anodes produced large amounts of ammonia, hydrogen and nitrogen (Fig. 17). This behavior was explained by different processes taking place on low and high surface catalysts. It was suggested that on platinum catalysts with low surface area, the dominant process is electrocatalytic oxidation of hydrazine, whereas on the Pt(HSSA), the catalytic decomposition of N_2H_4 is the main reaction (see Eqs. (5) and (6)).

$$N_2H_4 \rightarrow N_2 + 2H_2 \quad (5)$$

$$3N_2H_4 \rightarrow N_2 + 4NH_3 \quad (6)$$

Such a distribution of the products on both catalysts can also be explained by low activity of Pt(LSSA) towards hydrazine oxidation, leading to the release of a large amount of unreacted N_2H_4, while Pt(LSSA) almost fully utilizes the fuel. Nitrogen and ammonia were also detected at the cathode (Fig. 17). The presence of N_2 is related to cathode oxidation of N_2H_4 permeated through the membrane, and the amount of nitrogen is higher in the case of Pt(LSSA) due to low

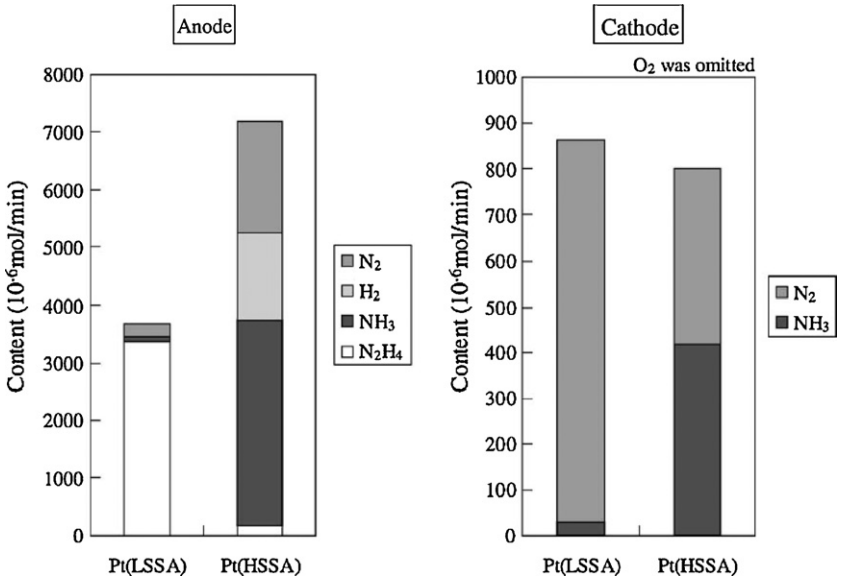

Fig. 17. The content of exhaust gases from electrodes with high and low specific surface area anode catalysts. Loading: anode (Pt 2 mg cm^{-2}), cathode (Pt 3 mg cm^{-2}), anode/cathode pressures = 0.1/0.1 MPa. Reproduced from [47] with permission from Elsevier.

fuel utilization on this catalyst. NH_3 cannot be oxidized or decomposed at the cathode given the present experimental conditions. It should be noted that values for open circuit voltage of studied fuel cells were considerably lower than theoretical ones. The possible explanation suggested by the authors is negative effect of products of decomposition, such as hydrogen [47]. The main conclusion from this work was that hydrazine easily permeates Nafion™ cation-exchange membranes, and only catalysts promoting electrooxidation of N_2H_4 are needed. The influence of different anode catalysts on the DHFC performance was also investigated in the same group [46]. Several noble metals with reduced surface area were tested, including Pt: 6.3 m^2 g^{-1}, Pd: 5.9 m^2 g^{-1}, Ru: 8.3 m^2 g^{-1} and Rh: 10.2 m^2 g^{-1} (Fig. 18). Fig. 18 shows that the highest OCV and cell performance at low overpotentials (below 50 mA cm^{-2}) were achieved using Pt and Pd catalysts, while the best performance at high overpotentials was obtained with rhodium catalysts. Ruthenium was the worst performing anode material. The evaluation of exhausted gases from both the anode and the cathode are shown in Figs. 19 and 20, respectively. The data obtained are in good agreement with those published earlier [47]. The authors suggested that the rate of catalytic decomposition of N_2H_4 on different noble catalysts is Ru > Rh > Pd > Pt [46]. A large amount of nitrogen produced at the cathode confirmed the observation that crossover of hydrazine through the Nafion™ cation-exchange membrane exists and negatively affects the total DHFC performance. Yamada et al. investigated the possible application of an anion-exchange membrane (AEM) in the direct hydrazine fuel cells [48]. The authors used an MEA based on Tosflex® SF-17 (currently commercially unavailable) with both platinum anode and cathode catalysts and compared it to a conventional cation-exchange membrane (CEM) MEA. The electroless plating method was used to attach catalysts to the membrane surface. The analysis of the exhaust gases from the cathode of the CEM MEA shows significant hydrazine crossover, as found before by the same research group [46,47]. The MEA based on the anion-exchange membrane shows significant resistance to N_2H_4 crossover, and the amount of hydrazine on the cathode was on the level of the detection limits.

A comparative study of CEM MEA and AEM MEA with composite anode [nickel powder (INCO 210), carbon-supported palladium catalyst (10% Pd on Vulcan XC-72, E-Tek Co.) and surface-treated

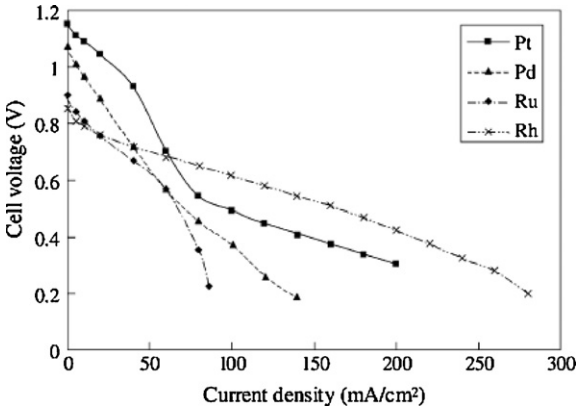

Fig. 18. Effect of the anode noble catalyst on the performance of the direct hydrazine fuel cell. Loading of anode/cathode (Pt/C 60 wt%) catalysts = 2/3 mg cm^{-2}. Reproduced from [46] with permission from Elsevier.

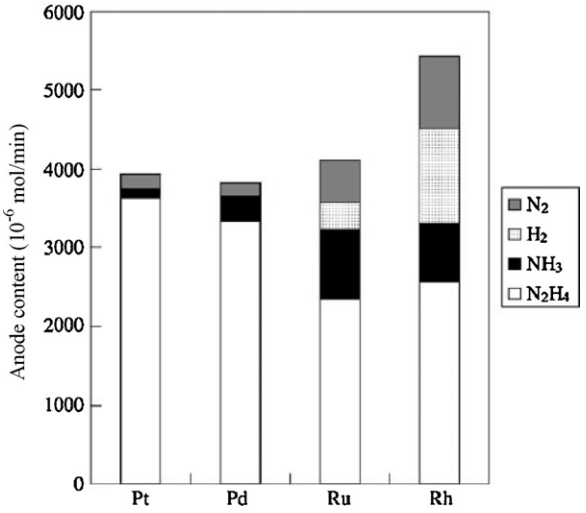

Fig. 19. The content of exhaust materials from the anode electrode with different anode catalysts. Current density = 20 mA cm^{-2}, anode/cathode pressures = 0.1/0.1 MPa. Reproduced from [46] with permission from Elsevier.

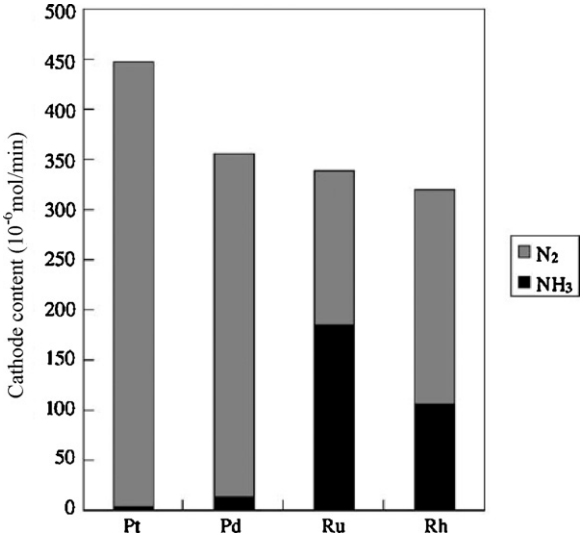

Fig. 20. The content of exhaust materials from the cathode electrode with different anode catalysts. Current density = 20 mA cm^{-2}, anode/cathode pressures = 0.1/0.1 MPa. Reproduced from [46] with permission from Elsevier.

Zr–Ni alloy] was performed by Li and co-workers [66]. Either a mixture of sodium borohydride and hydrazine or pure hydrazine was used. MEA constructed on an anion-exchange membrane shows significantly higher power density than MEA constructed on a cation-exchange membrane, yielding such values as 92 against 64 mW cm^{-2} (Figs. 21 and 22). This observation can be explained by the decrease in hydrazine crossover followed by a reduction in parasitic current loss, due to oxidation of permeated N_2H_4 on cathode side.

The influence of NaOH addition to N_2H_4 fuel for both anion- and cation-exchange MEA was studied in the same group [56]. The same composite anode material as in [71] (Zr–Ni alloy) was used for MEA fabrication. The MEAs using alkaline hydrazine solution demonstrated high power densities of 84 and 73.9 mW cm^{-2} for AE and CE membranes, respectively (Fig. 23). The addition of NaOH influenced the suppression of N_2H_4 hydrolysis, decreasing the concentration of $N_2H_5^+$ in the solution and as a result, hindering the hydrazine crossover through the membrane. The performance of

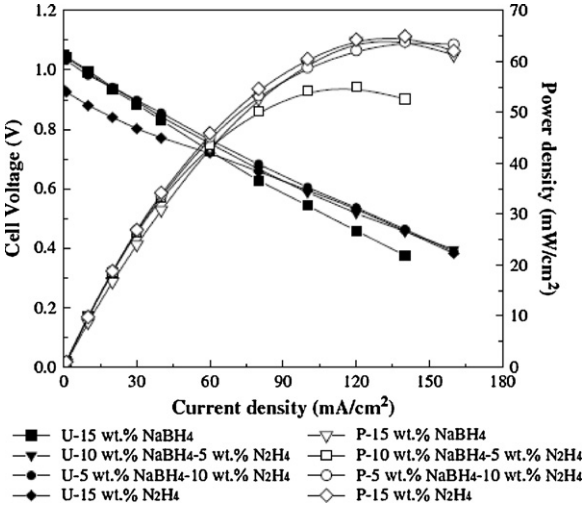

Fig. 21. Cell voltage and power density vs. current density for fuel cells using alkaline $NaBH_4$–N_2H_4 solutions as the fuel with CEM [70]. (Cathode: Pt 1 mg cm^{-2}, dry O_2 at a flow rate of 150 mL min^{-1} (1 atm); anode: composite catalyst 10 mg cm^{-2}). Reproduced from [66] with permission from Elsevier.

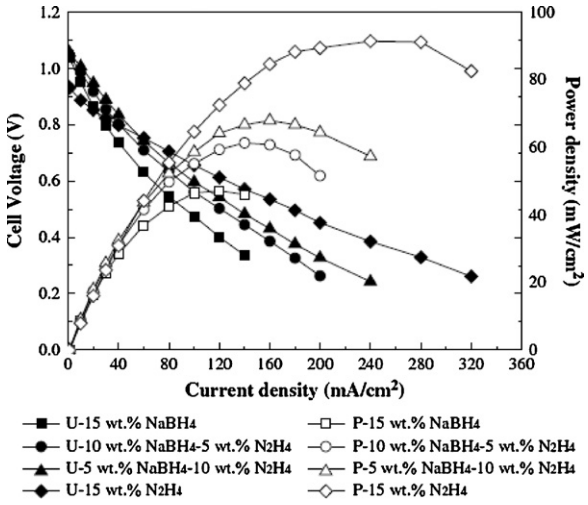

Fig. 22. Cell voltage and power density vs. current density for the fuel cells using alkaline $NaBH_4$–N_2H_4 solutions as the fuel with AEM. (Cathode: Pt 1 mg cm^{-2}, dry O_2 at a flow rate of 150 mL min^{-1} (1 atm); anode: composite catalyst 10 mg cm^{-2}). Reproduced from [66] with permission from Elsevier.

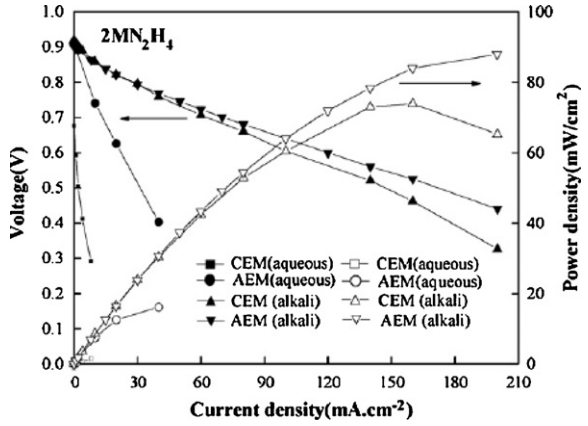

Fig. 23. Effect of NaOH in addition to aqueous hydrazine solution on the performance of the DHFC at room temperature. Anolyte: 2 M N_2H_4 or 2 M N_2H_4 + 4 M NaOH. Fuel flow: 5 mL min^{-1}, O_2 flow: 150 mL min^{-1} (0.1 MPa). Reproduced from [56] with permission from Elsevier.

DHFC with an anion-exchange membrane was higher than that of CEM, confirming the superior properties of AEM in the suppression of fuel permeation.

Based on the results discussed in the previous chapter, the electrooxidation of hydrazine in alkaline media occurs with full fuel utilization, and can be performed even with non-noble catalysts. The results obtained in [46–48,56,66] show that DHFC operated better with the alkaline membrane. This information encourages investigation of MEAs based on Pd, Ag and Au anode catalysts with AEM. Such a combination should lead to increased performance of AEM DHFC when compared to conventional CEM fuel cells.

Recently the new type of DHFC using H_2O_2 as an oxidizer was investigated [61]. The MEA was fabricated using Nafion^{TM} 112 membrane, Au/C cathode and composite Ni-Pt/C anode catalysts for hydrazine oxidation. It was found that a maximum power density of 1.02 W cm^{-2} can be achieved by using alkaline N_2H_4 solution as the fuel and acidic H_2O_2 solution as the oxidizer at 80 °C. However, taking into account the high oxidative and corrosive nature of H_2O_2 additional experiments studying the durability of MEA and DHFC should be performed.

4. Conclusions

The lack of carbon atoms in hydrazine, resulting in zero emission of CO_2 to the atmosphere, makes it a unique fuel for direct fuel cells. It is also a liquid and can be easily stored and transferred through existing supply chains. Hydrazine is a simple molecule with high theoretical power density, and it can be electrooxidized on the surface of many catalysts via mechanisms leading only to nitrogen and water. The electrooxidation of N_2H_4 was intensively studied by many researchers, leading to a better understanding of the processes taking place on the surface of catalysts. Several metals were found as possible candidates on anodes for direct hydrazine fuel cells, such as Ag, Pd and Pt. However, there is a significant gap between the investigation of many of these catalysts towards hydrazine electrooxidation and tests of these materials in real MEA composites. Only several noble metals and Ni–Zr alloys were investigated under MEA operation conditions. This gap can be explained by the poor performance of DHFC based on readily available cation-exchange membranes, due to parallel N_2H_4 decomposition in acidic media and high fuel crossover from the anode to the cathode. This problem can be solved by using anion-exchange membranes, and a number of reviewed works have proposed significant improvement of fuel cells based on AEM. Currently, only a few manufacturers produce anion-exchange membranes suitable for the fuel cell industry. In our opinion, the development and commercialization of AEM is the crucial step for a breakthrough in the DHFC research. A step-by-step improvement in the electrocatalysts for hydrazine oxidation, membrane fabrication, MEA synthesis and fuel cell design will lead to an overall implementation of direct hydrazine fuel cells.

References

[1] K. Scott, W. Taama, J. Cruickshank, J. Power Sources 65 (1997) 159–171.
[2] X. Ren, P. Zelenacy, S. Thomas, J. Davey, S. Gottesfeld, J. Power Sources 86 (2000) 111–116.
[3] A. Heinzel, V.M. Barragan, J. Power Sources 84 (1999) 70–74.
[4] V. Baglio, A.S. Aricò, A. Di Blasi, V. Antonucci, P.L. Antonucci, S. Licoccia, E.S. Fiory, Electrochim. Acta 50 (2005) 1241–1246.
[5] H. Dohle, J. Divisek, J. Mergel, H.F. Oetjen, C. Zingler, D. Stolten, J. Power Sources 105 (2002) 274–282.
[6] X. Ren, T.E. Springer, T.A. Zawodzinski, S. Gottesfeld, J. Electrochem. Soc. 147 (2) (2000) 466–474.
[7] Z. Jusys, T.J. Schmidt, L. Dubau, K. Lasch, L. Jorissen, J. Garche, R.J. Behm, J. Power Sources 105 (2002) 297–304.
[8] Y. Morimoto, E.B. Yeager, J. Electroanal. Chem. 444 (1998) 95–100.
[9] H. William, L.-V.A. Paganin, E.R. Gonalez, Electrochim. Acta 47 (2002) 3715–3722.
[10] Q. Fan, C. Pu, E.S. Smotkin, J. Electrochem. Soc. 143 (1996) 3053–3057.
[11] W.-F. Lin, J.-T. Wang, R.F. Savinell, J. Electrochem. Soc. 144 (1997) 1917–1922.
[12] H. Houa, G. Suna, R. Heb, Z. Wu, B. Sun, J. Power Sources 182 (2008) 95–99.
[13] K. Bergamaski, E.R. Gonzalez, F.C. Nart, Electrochim. Acta 53 (2008) 4396–4406.
[14] E. Ribadeneira, B.A. Hoyos, J. Power Sources 180 (2008) 238–242.
[15] A. Ghumman, P.G. Pickup, J. Power Sources 179 (2008) 280–285.
[16] H. Songa, X. Qiu, D. Guob, F. Li, J. Power Sources 178 (2008) 97–102.
[17] Q. Wang, G.Q. Suna, L. Cao, L.H. Jiang, G.X. Wang, S.L. Wang, S.H. Yang, Q. Xin, J. Power Sources 177 (2008) 142–147.
[18] X. Xue, J. Ge, T. Tian, C. Liu, W. Xing, T. Lua, J. Power Sources 172 (2007) 560–569.
[19] M. Nie, H. Tang, Z. Wei, S.P. Jiang, P.K. Shen, Electrochem. Commun. 9 (2007) 2375–2379.
[20] E. Antolini, J. Power Sources 170 (2007) 1–12.
[21] H. Wang, C. Xu, F. Cheng, S. Jiang, Electrochem. Commun. 9 (2007) 1212–1216.
[22] R. Chetty, K. Scott, Electrochim. Acta 52 (2007) 4073–4081.
[23] A. Serov, C. Kwak, Appl. Catal. B: Environ. 91 (2009) 1–10.
[24] K.-D. Cai, G.-P. Yin, J. Zhang, Z.-B. Wang, C.-Y. Du, Y.-Z. Gao, Electrochem. Commun. 10 (2008) 238–241.
[25] J.-Y. Im, B.-S. Kim, H.-G. Choi, S.M. Cho, J. Power Sources 179 (2008) 301–304.
[26] S. Ueda, M. Eguchi, K. Uno, Y. Tsutsumi, N. Ogawa, Solid State Ionics 177 (2006) 2175–2178.
[27] M.M. Mench, H.M. Chance, C.Y. Wang, J. Electrochem. Soc. 151 (2004) A144–A150.
[28] Y. Liu, M. Muraoka, S. Mitsushima, K.-I. Ota, N. Kamiya, Electrochim. Acta 52 (2007) 5781–5788.
[29] L. Lu, G. Yin, Y. Tong, Y. Zhang, Y. Gao, M. Osawa, S. Ye, J. Electroanal. Chem. 619–620 (2008) 143–151.
[30] Y. Zhang, Le. Lu, Y. Tong, M. Osawa, S. Ye, Electrochim. Acta 53 (2008) 6093–6103.
[31] J.-H. Yoo, H.-G. Choi, C.-H. Chung, S.M. Cho, J. Power Sources 163 (2006) 103–106.
[32] Y. Liu, S. Mitsushima, K. Ota, N. Kamiya, Electrochim. Acta 51 (2006) 6503–6509.
[33] J.-H. Yu, H.-G. Choi, S.M. Cho, Electrochem. Commun. 7 (2005) 1385–1388.
[34] G. Kerangueven, C. Coutanceau, E. Sibert, J.-M. Léger, C. Lamy, J. Power Sources 157 (2006) 318–324.
[35] Q. Zhang, Z. Li, S. Wang, W. Xing, R. Yu, X. Yu, Electrochim. Acta 53 (2008) 8298–8304.
[36] I. Mizutani, Y. Liu, S. Mitsushima, K. Ota, N. Kamiya, J. Power Sources 156 (2006) 183–189.
[37] X. Yua, P.G. Pickup, J. Power Sources 182 (2008) 124–132.
[38] A. Serov, C. Kwak, Appl. Catal. B: Environ. 90 (2009) 313–320.
[39] A.A. Serov, S.-Y. Cho, S. Han, M. Min, G. Chai, K.H. Nam, C. Kwak, Electrochem. Commun. 9 (2007) 2041–2044.
[40] A.A. Serov, M. Min, G. Chai, S. Han, S. Kang, C. Kwak, J. Power Sources 175 (2008) 175–182.
[41] A.A. Serov, C. Kwak, Catal. Commun. 10 (2009) 1551–1554.
[42] A.A. Serov, M. Min, G. Chai, S. Han, S.J. Seo, Y. Park, H. Kim, C. Kwak, J. Appl. Electrochem. 39 (2009) 1509–1516.
[43] A. Serov, T. Nedoseykina, O. Shvachko, C. Kwak, J. Power Sources 195 (2010) 175–180.
[44] A. Serov, C. Kwak, Appl. Catal. B: Environ. doi:10.1016/j.apcatb.2010.04.011.
[45] J. Ma, N.A. Choudhury, Y. Sahai, Renew. Sustain. Energy Rev. 14 (2010) 183–199.
[46] K. Yamada, K. Yasuda, H. Tanaka, Y. Miyazaki, T. Kobayashi, J. Power Sources 122 (2003) 132–137.
[47] K. Yamada, K. Asazawa, K. Yasuda, T. Ioroi, H. Tanaka, Y. Miyazaki, T. Kobayashi, J. Power Sources 115 (2003) 236–242.
[48] K. Yamada, K. Yasuda, N. Fujiwara, Z. Siroma, H. Tanaka, Y. Miyazaki, T. Kobayashi, Electrochem. Commun. 5 (2003) 892–896.
[49] G. Gao, D. Guo, C. Wang, H. Li, Electrochem. Commun. 9 (2007) 1582–1586.
[50] J. Li, X. Lin, Sens. Actuators B 126 (2007) 527–535.
[51] Q. Yi, L. Li, W. Yu, Z. Zhou, G. Xu, J. Mol. Catal. A: Chem. 295 (2008) 34–38.
[52] G.-W. Yang, G.-Y. Gao, C. Wang, C.-L. Xu, H.-L. Li, Carbon 46 (2008) 747–752.
[53] W. Ye, B. Yang, G. Cao, L. Duan, C. Wang, Thin Solid Films 516 (2008) 2957–2961.
[54] B. Dong, B.-L. He, J. Huang, G.-Y. Gao, Z. Yang, H.-L. Li, J. Power Sources 175 (2008) 266–271.
[55] V. Rosca, M.T.M. Koper, Electrochim. Acta 53 (2008) 5199–5205.
[56] W.X. Yin, Z.P. Li, J.K. Zhu, H.Y. Qin, J. Power Sources 182 (2008) 520–523.
[57] C. Tan, F. Wang, J. Liu, Y. Zhao, J. Wang, L. Zhang, K.C. Park, M. Endo, Mater. Lett. 63 (2009) 969–971.
[58] L. Chen, G. Hu, G. Zou, S. Shao, X. Wang, Electrochem. Commun. 11 (2009) 504–507.
[59] Y. Shen, Q. Xu, H. Gao, N. Zhu, Electrochem. Commun. 11 (2009) 1329–1332.
[60] Q. Yi, W. Yu, J. Electroanal. Chem. 633 (2009) 159–164.
[61] S.J. Lao, H.Y. Qin, L.Q. Ye, B.H. Liu, Z.P. Li, J. Power Sources 195 (2010) 4135–4138.
[62] G. Karim-Nezhad, R. Jafarloo, P.S. Dorraji, Electrochim. Acta 54 (2009) 5721–5726.
[63] K. Asazawa, K. Yamada, H. Tanaka, M. Taniguchi, K. Oguro, J. Power Sources 191 (2009) 362–365.
[64] Y. Wang, Y. Wan, D. Zhang, Electrochem. Commun. 12 (2010) 187–190.
[65] Y. Lin, R. Ran, Y. Guo, W. Zhou, R. Cai, J. Wang, Z. Shao, Int. J. Hydrogen Energy 35 (2010) 2637–2642.
[66] H. Qin, Z. Liu, Y. Guo, Z. Li, Int. J. Hydrogen Energy 35 (2010) 2868–2871.
[67] M.R. Andrew, W.J. Gressler, J.K. Johnson, R.T. Short, K.R. Williams, J. Appl. Electrochem. 2 (1972) 327.
[68] K. Tamura, T. Kahara, J. Electrochem. Soc. 123 (1976) 776.
[69] L.J.M.J. Blomen, M.N. Mugerwa, Fuel Cell Systems, 1993, ISBN 0-306-44158-6.
[70] H. Qin, Z. Liu, W. Yin, J. Zhu, Z. Li, J. Power Sources 185 (2008) 895–988.
[71] Z.P. Li, B.H. Liu, J.K. Zhu, S. Suda, J. Power Sources 163 (2006) 555.
[72] K. Asazawa, K. Yamada, H. Tanaka, A. Oka, M. Taniguchi, T. Kobayashi, Angew. Chem. Int. Ed. 46 (2007) 8024–8027.